JOURNAL OF MOLECULAR SPECTROSCOPY 125, 225–232 (1987)

Excited State Magnetic Hyperfine Interactions in Gas Phase Strontium and Calcium Monohydrides

TIMOTHY C. STEIMLE, TIMOTHY P. MEYER, AND YAHYA AL-RAMADIN

Department of Chemistry, Arizona State University, Tempe, Arizona 85287

AND

PETER BERNATH

Department of Chemistry, University of Arizona, Tucson, Arizona 85721

Numerous rotational lines in the $B^2\Sigma^+(v' = 0)$–$X^2\Sigma^+(v'' = 0)$ band system of CaH and the $A^2\Pi_{1/2}(v' = 0)$–$X^2\Sigma(v'' = 0)$ subband system of SrH have been recorded at sub-Doppler resolution using the technique of intermodulated fluorescence. The recorded spectra exhibit a small splitting associated with magnetic hyperfine interactions in both the ground and the excited electronic states. An analysis of the excited state contributions was performed and the results were interpreted in terms of the possible nature of the electronic wavefunction. The results suggest that the effective Hamiltonian needs to be modified in order to give qualitative agreement for the Λ-doubling type magnetic hyperfine parameter. The determined hyperfine parameters for the $B^2\Sigma^+$ state are consistent with the current theoretical interpretation of the nature of this state.

I. INTRODUCTION

The group IIA (Mg, Ca, Sr, and Ba) hydrides and halides have played an important role in the development of molecular spectroscopy and quantum chemistry. These compounds are characterized by strong visible transitions whose associated energy level pattern can be attributed to spin–orbit, spin–rotation, and magnetic hyperfine interactions. In addition, a low-lying state in the hydrides is thought to exhibit a double minimum potential surface (*1, 2*). These molecules are responsible for notable features in stellar emission spectra (*3*) and have been the subject of interstellar molecular searches (*4*).

The nature of the low-lying electronic states of the group IIA halides and hydrides are roughly described as having an electron in a metal-centered hybridized atomic orbital outside the M^{++} and X^- filled orbitals. The hybridized orbital is primarily a linear combination of the *ns*, *np*, and $(n - 1)d$ atomic orbitals, where n is the largest principal quantum number for the highest energy occupied orbital of the metal. This simple one-electron model was initially employed in the interpretation of the matrix isolated ESR results (*5*) and has been modified to predict additional properties of the gas phase compound (*6–9*). Quantitative agreement among the simple one-electron model and detailed ab initio calculations (*10*) and experiments has been achieved for

0022-2852/87 $3.00

the halides but lack of pertinent experimental data has limited the comparisons for the hydrides.

An analysis of magnetic hyperfine effects, which are a consequence of the interaction of any nonzero nuclear spin angular momentum with nonzero electronic angular momentum, provides a particularly sensitive means of testing the electronic models. Here we report on the results of an analysis of the features in the $A^2\Pi_{1/2}(v' = 0)$–$X^2\Sigma^+(v'' = 0)$ subband system of SrH and the $B^2\Sigma^+(v' = 0)$–$X^2\Sigma^+(v'' = 0)$ band system of CaH recorded with sub-Doppler resolution and an interpretation of the excited state magnetic hyperfine interactions. Recent spectroscopic studies of gas phase CaH include the rotational analysis of the emission spectrum (*11*) and the laser-excited fluorescence study of perturbations in the $A^2\Pi$ and $B^2\Sigma^+$ states (*12*). Recently, the gas phase visible emission spectrum of SrH has been recorded by Fourier transform spectroscopy and a deperturbation of the $A^2\Pi/B^2\Sigma^+$ interactions was performed (*13*). The matrix isolated ESR measurements for both SrH and CaH were obtained some time ago (*14*). A detailed SCF–CISD calculation for CaH has also been reported (*15*).

II. EXPERIMENTAL DETAILS

The alkaline earth monohydrides were produced in a flowing gas reaction chamber via the reaction of the metal vapor with anhydrous formic acid. The metal vapor was generated by resistively heating the solid metal sample in the presence of an argon carrier gas. The total pressure in the reaction chamber was maintained at $\sim$1.5 Torr with a flow rate of a few liters/sec. Under these conditions a weak reddish chemiluminescence was observed which, when dispersed, could be attributed to the hydride and hydroxide compounds (*16*). The ratio of the hydride to hydroxide chemiluminescence was greatly reduced if a small amount of water was introduced into the reaction chamber.

The optical arrangement for the intermodulated fluorescence (IMF) experiments has been given previously (*17*). Briefly, the output from a continuous wave dye laser was divided into two portions of nearly equal intensity and counter propagated colinearly through the sample. Each portion of the beam was amplitude modulated and a signal at the sum of the modulation frequencies was sought in the laser-exited fluorescence. The SrH experiments were recorded in the early stages of the research with a Coherent Model 699-29 dye laser operating with Pyridine and pumped with 6 W of 488-nm radiation producing 250 mW of tunable radiation in the 745- to 751-nm spectral range. The wavelengths of the radiation were determined with the internal wavemeter of the laser system. The CaH measurements were recorded with a Coherent Model 699-21 dye laser operating DCM and pumped with 5 W of 488-nm radiation which produced 250 mW of tunable radiation in the desired 627- to 635-nm spectral region. The absolute wavelength calibration for the CaH measurements was made by simultaneously recording the I_2 absorption spectrum (*18*). In both sets of experiments, the transmission of a 1-m thermally stabilized confocal etalon, whose FSR had been calibrated by measuring the sub-Doppler I_2 features (*19*), was used to measure relative frequency changes. In the SrH measurements, the IMF and etalon transmission signals were recorded and stored with the associated data processing system of the laser. In the CaH measurements, the IMF, etalon transmission, and I_2 absorption signals were recorded and processed with a laboratory microcomputer.

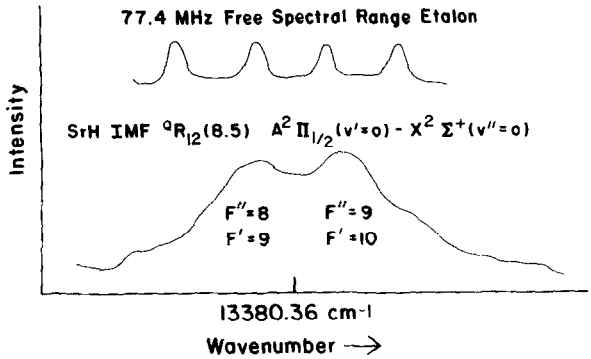

FIG. 1. The $^{Q}R_{12}(8.5)$ branch feature in the $A^2\Pi_{1/2}(v' = 0)$–$X^2\Sigma^+(v'' = 0)$ subband of SrH as measured by intermodulated fluorescence. The small splitting is due to the proton magnetic hyperfine interactions.

III. OBSERVATIONS AND DATA REDUCTION

A total of 24 features in the $A^2\Pi_{1/2}(v' = 0)$–$X^2\Sigma^+(v'' = 0)$ subband of SrH and 12 features in the $B^2\Sigma^+(v' = 0)$–$X^2\Sigma^+(v'' = 0)$ band system of CaH were recorded at sub-Doppler resolution. In Figs. 1 and 2 the IMF and etalon transmission signals for the $^{Q}R_{12}(8.5)$ branch feature of SrH and the $R_2(5.5)$ branch feature for CaH are illustrated and represent typical recordings. The two partially resolved lines are a result of a splitting of the energy levels associated with the branch features arising from the magnetic hyperfine interaction between the unpaired electron and the proton nuclear spin ($I = \frac{1}{2}$). The quantum number assignments were straightforward based on the Doppler-limited analyses (*20, 21*) and the relative intensities of the two peaks.

The linewidths were laser-power dependent and the laser beam was slightly defocused in the CaH measurements to produce better resolution. A deconvolution process using two Lorentzian lineshapes with adjustable intensities and relative positions was used

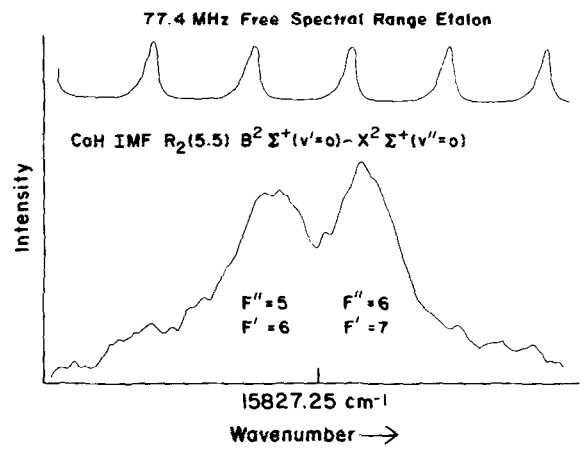

FIG. 2. The $R_2(5.5)$ branch feature in the $B^2\Sigma^+(v' = 0)$–$X^2\Sigma^+(v'' = 0)$ band of CaH as measured by intermodulated fluorescence. The small splitting is due to the proton magnetic hyperfine interactions.

to accurately determine the splitting of the hyperfine components of the line. Linewidths of 85 MHz (FWHM) for SrH and 70 MHz (FWHM) for CaH were used in the deconvolution. The determined quantum number assignments and the difference between observed and calculated splittings are presented in Table I and Table II for SrH and CaH, respectively.

The measured features are not known to be heterogeneously perturbed and therefore an effective Hamiltonian approach was used as described previously (*22*). The magnetic hyperfine contributions to the Hamiltonian are

$$H_{\text{hfs}} = aI_zL_z + b_F\mathbf{I}\cdot\mathbf{S} + 1/3c(3I_zS_z - \mathbf{I}\cdot\mathbf{S}) - 1/2d(S_+I_+ + S_-I_-), \quad (1)$$

TABLE I

Hyperfine Splitting of Features in the $A^2\Pi_{1/2}(v' = 0)$–$X^2\Sigma^+(v'' = 0)$ Subband System of SrH as Measured by IMF

Optical Branch Line	Assignment[a] Lower F'	F"	Upper F'	F"	Observed Splitting (MHz)	Obs-calc[b] (MHz)
$P_1(1.5)$	2	3	1	2	109	-5
$P_1(2.5)$	3	4	2	3	105	-5
$P_1(3.5)$	4	5	3	4	118	10
$P_1(5.5)$	6	7	5	6	122	18
$P_1(7.5)$	8	9	7	8	100	-4
$P_1(10.5)$	11	12	10	11	102	-1
$P_1(11.5)$	12	13	11	12	107	5
$P_1(14.5)$	15	16	14	15	103	1
$P_1(15.5)$	16	17	15	16	83	-17
$P_1(17.5)$	18	19	17	18	124	24
$P_1(18.5)$	19	20	18	19	92	-7
$P_{Q12}(1.5)$	1	1	2	2	113	20
$P_{Q12}(2.5)$	2	2	3	3	76	-18
$P_{Q12}(3.5)$	3	3	4	4	80	-15
$P_{Q12}(5.5)$	5	5	6	6	89	-7
$Q_1(0.5)$	1	1	0	0	158	-12
$Q_1(2.5)$	3	3	2	2	100	-12
$Q_1(13.5)$	14	14	13	13	98	-3
$Q_{R12}(1.5)$	2	1	3	2	107	16
$Q_{R12}(2.5)$	3	2	4	3	95	2
$Q_{R12}(3.5)$	4	3	5	4	89	-5
$Q_{R12}(8.5)$	9	8	10	9	92	-4
$Q_{R12}(12.5)$	13	12	14	13	116	20
$R_1(2.5)$	4	3	3	2	125	13
RMS						7 MHz

[a] Total angular momentum quantum number assignment: "Lower" (Upper) refers to the lowest (highest) frequency components of the spectral features (see Figure 1).
[b] Results from fit to excited state magnetic hyperfine constants. All other parameters held fixed.

TABLE II

Hyperfine Splitting of Features in the $B^2\Sigma^+(v' = 0)$–$X^2\Sigma^+(v'' = 0)$ Band System of CaH as Measured by IMF

Optical Branch Line	Assignment[a] Lower F'	F"	Upper F'	F"	Observed Splitting (MHz)	Obs-calc[b] (MHz)	Obs-calc[c] (MHz)
$P_1(1.5)$	1	2	0	1	92.8	-3.8	5.2
$P_1(2.5)$	2	3	1	2	98.5	6.5	9.9
$P_1(5.5)$	5	6	4	5	86.8	-1.0	3.2
$P_1(6.5)$	6	7	5	6	89.3	2.1	3.1
$P_1(7.5)$	7	8	6	7	86.9	0.0	1.7
$P_2(5.5)$	4	5	5	6	80.9	-1.5	-3.0
$P_2(6.5)$	5	6	6	7	81.0	-1.0	-2.1
$P_2(7.5)$	6	7	7	8	79.1	-0.5	-5.2
$R_1(1.5)$	3	2	2	1	109.2	6.4	9.8
$R_1(5.5)$	7	6	6	5	88.8	0.1	1.4
$R_2(1.5)$	2	1	3	2	74.5	-1.4	-3.8
$R_2(5.5)$	6	5	7	6	80.8	0.6	-1.8
RMS =						4 MHz	5 MHz

[a] Total angular momentum quantum number assignment: "Lower" (Upper) refers to the lowest (highest) frequency components of the spectral features (see Figure 2).

[b] Results from a fit to excited state magnetic hyperfine constants b_F and c. All other parameters held fixed.

[c] Results from fit to excited state magnetic hyperfine constant c. All other parameters held fixed.

where a, b_F, c, and d are the orbital, Fermi contact, dipolar, and Λ-doubling type magnetic hyperfine constants, respectively (*23*). All four contributions are nonzero for a $^2\Pi$ state while only the Fermi contact and dipolar terms exist for a $^2\Sigma^+$ state. The hyperfine constants are related to the electronic wavefunctions through the expectation value expressions

$$a/Hz = \mu_0/4\pi h \sum_i 2\mu_B g_N \mu_N \langle r_i^{-3} \rangle_l, \tag{2}$$

$$b_F/Hz = \mu_0/h \sum_i g_i \mu_B g_N \mu_N \langle \phi_i \delta(r_i) \rangle_s, \tag{3}$$

$$c/Hz = \mu_0/4\pi h \sum_i \tfrac{3}{2} g_i \mu_B g_N \mu_N \langle \phi_i (3\cos^2\theta_i - 1)/r_i^3 \rangle_s, \tag{4}$$

$$d/Hz = \mu_0/4\pi h \sum \tfrac{3}{2} g_i \mu_B g_N \mu_N \langle \phi_i (\sin^2\theta_i/r_i^3) \rangle_s, \tag{5}$$

in the usual notation with $\phi = \mathbf{s}_i \cdot \mathbf{S}/S(S+1)$ and θ_i an r_i are the spherical polar coordinates of the open shell electrons with respect to the nuclei with nonzero spin. The Fermi contact term is designated as b_F. The subscripts l and s on the expectation values denote the fact that the spin and orbital angular momentum are not necessarily carried by the same electron.

A nonlinear least-squares fitting procedure was developed which determines energies based on estimated hyperfine parameters, calculates the splittings, and predicts corrections to the initial estimates of the parameters. For computational simplicity, all calculations were performed in a case a_β basis set. The complete 4×4 matrix for the $^2\Sigma^+$ state and 8×8 matrix for the $^2\Pi$ state for each possible F value was constructed and diagonalized. Initially, it was assumed that the splitting of the optical branch features was solely a result of the interactions in the ground electronic state. A fit of the data to this model produced reasonably good results as judged by the rms deviation but with values of $b_F = 191(10)$ MHz and $b_F = 169(8)$ MHz for SrH and CaH, respectively, which compare poorly with the matrix isolated values (*8*) of $b_F = 122$ and $b_F = 135$ MHz. A closer examination of the spectra for branch features which connect to common levels in the ground state indicated that there were systematic differences. In addition, the recent gas phase results for MgH (*24*) would indicate that the matrix shift for the group IIA hydrides is small. Therefore, the ground state magnetic hyperfine parameters were held fixed to the values determined from the ESR data and excited hyperfine parameters were determined. The quality of the data is insufficient to simultaneously determine all of the constants. Various one- and two-parameter fits were performed. The results are presented in Table III.

The a, b_F, and c contributions to the hyperfine energies for a $^2\Pi_{1/2}$ spin–orbit component rapidly decrease as a function of increasing rotational angular momentum, whereas the d contribution remains nearly constant. Therefore, it was necessary to include d in the fits. Inclusion of additional parameters did not substantially improve the quality of the fit of the SrH data. A two-parameter fit of the CaH data was marginally accomplished, producing an error estimate for b_F which was larger than the determined value. The results would indicate that b_F is small and negative. As indicated by the large correlation coefficient for the two-parameter fit (>0.988), nearly comparable fits were obtained fitting to only b_F or c. The fit to c was preferred because of a slightly smaller variance. A fit to b_F produced a value of $-31(6)$ MHz.

IV. DISCUSSION

The hyperfine interactions in the $A^2\Pi_{1/2}$ and $B^2\Sigma^+$ states of SrH and CaH, respectively, are small, in qualitative agreement with the notion that the unpaired electron is in a nonbonding orbital centered on the alkaline earth nucleus (Table III). The negative d value is unexpected because all of the quantities in Eq. (5) are positive for a configuration with a single unpaired electron. Similar inconsistencies in sign were observed for the excited state of CuF (*25*), ScO (*26*), and BaI (*27*) while consistent values were determined for the ground states of CuO (*28*) and CH (*29, 30*). A possible explanation is that the "true" value of d is contaminated by higher-order terms which have the same quantum number dependence. The fact that the known discrepancies involve only excited states favor this explanation. An extension of the effective Hamiltonian to include such contributions is now underway.

TABLE III

Hyperfine Parameters for the $A^2\Pi(v' = 0)$ State for SrH and the $B^2\Sigma^+(v = 0)$ State of CaH[a]

SrH (MHz)	CaH (MHz)		
a -		Fit 1	Fit 2
b_F -	b_F	-9(17)	--
c -	c	74(20)	102(4)
d -95(12)			
		Correlation b_F	Matrix c
	b_F	1.00	0.988
	c	0.988	1.00

[a] The results of fitting the observed splitting to excited state hyperfine parameters holding fine structure and rotational parameter fixed to the gas phase optically determined values and the ground state hyperfine to those of the matrix isolated ESR determined values. The numbers in parentheses represent a 80% confidence estimate.

Quantitative interpretation of the $B^2\Sigma^+(v = 0)$ state hyperfine parameters is possible. The ab initio calculation (*15*) predicts that the important configurations for the $B^2\Sigma^+$ state are

$$6\sigma^2 8\sigma \tag{6}$$

$$6\sigma 7\sigma^2 \tag{7}$$

$$6\sigma 7\sigma 8\sigma, \tag{8}$$

with the 6σ orbital being essentially a $1s$ atomic orbital on H, the 7σ being the linear combination $4s(65\%)$, $4p(31\%)$, and $3d(1\%)$, and the 8σ being the linear combination $4s(4.3\%)$, $4p(23\%)$, and $3d(71\%)$ both centered on Ca. The relative weights of configurations 6, 7, and 8 are 0.92, 0.01, and 0.02, respectively. These values can be used along with the ground state atomic hydrogen Fermi contact parameter (1420 MHz) to predict a value of $\sim$35 MHz for $b_F(B^2\Sigma^+)$. Our analysis would indicate that $b_F(B^2\Sigma^+)$ is small and negative. Spin polarization contributions could explain the discrepancy.

A numerical calculation using a single zeta basis set that included an s-orbital, a set of p-orbital and a set of d-orbital functions to approximate the valence atomic orbitals of Ca was performed. The expectation value of the operator of Eq. (4) over these atomic basis sets was calculated for the internuclear distance fixed at the experimentally determined value (*11*). A $c(B^2\Sigma^+) \approx 115$ MHz is estimated when atomic expectation values were combined with the coefficients for the linear combination of the atomic orbitals (*15*) used to approximate the molecular orbital. This is in good agreement with the experimentally determined value ($c(B^2\Sigma^+) = 104(2)$ MHz).

Improvements in the resolution of the IMF technique or possibly the results of an excited state microwave-optical double-resonance experiment could produce well-determined magnetic hyperfine parameters for these molecules. The demonstrated method of production of the alkaline earth monohydrides with formic acid is well

suited for future spectroscopic investigations because of the relatively low temperatures and pressures.

ACKNOWLEDGMENTS

This research was supported by grants from Research Corporation and the Arizona State University Faculty Grants-in-Aid program. We thank Professor Balasubramanian and Mr. Doug Chapman for assisting in the numerical calculation of the CaH dipolar parameter.

RECEIVED: March 5, 1987

REFERENCES

1. L. KLYNNING AND H. MARTIN, *J. Phys. B* **14,** L365–L366 (1981).
2. W. J. BALFOUR AND H. M. CARTWRIGHT, *Chem. Phys. Lett.* **32,** 82–85 (1975).
3. B. BARBUY, *Astron. Astrophys.* **151,** 189–197 (1985).
4. J. BLACK, P. BERNATH, T. C. STEIMLE, AND B. TURNER, private communication.
5. W. WELTNER, JR., "Magnetic Atoms and Molecules," Van Norstrand–Reinhold, Princeton, NJ, 1983.
6. L. KLYNNING AND H. MARTIN, *Phys. Scr.* **20,** 594–598 (1979).
7. S. RICE, H. MARTIN, AND R. W. FIELD, *J. Chem. Phys.* **82,** 5023–5034 (1985).
8. P. F. BERNATH, B. PINCHEMEL, AND R. W. FIELD, *J. Chem. Phys.* **74,** 5508–5515 (1981).
9. T. TÖRRING, W. E. ERNST, AND S. KINDT, *J. Chem. Phys.* **81,** 4614–4619 (1984).
10. N. HONJOU, G. F. ADAMS, AND D. R. YARKONY, *J. Chem. Phys.* **79,** 4376–4381 (1983).
11. L. E. BERG AND L. KLYNNING, *Phys. Scr.* **10,** 331–336 (1974).
12. H. MARTIN, *J. Mol. Spectrosc.* **108,** 66–81 (1984).
13. L. B. KNIGHT, JR., AND W. WELTNER, JR., *J. Chem. Phys.* **54,** 3875–3884 (1971).
14. O. APPELBLAD, L. KLYNNING, AND J. W. C. JOHNS, *Phys. Scr.* **33,** 415–419 (1986).
15. N. HONJOU, T. NORO, M. TAKAGI, K. OHNO, AND M. MAKITA, *J. Phys. Soc. Jpn.* **48,** 586–590 (1980).
16. C. R. BRAZIER, P. F. BERNATH, S. KINSEY-NIELSEN, AND L. C. ELLINGBOE, *J. Chem. Phys.* **82,** 1043–1045 (1985).
17. T. C. STEIMLE AND Y. AZUMA, *J. Mol. Spectrosc.* **118,** 237–247 (1986).
18. S. GERSTENKORN AND P. LUC, "Atlas du Spectre d'Absorption de la Molecule d'Iode," Centre National de la Recherche Scientifique, Paris, France, 1978; *Rev. Phys. Appl.* **14,** 791–796 (1979).
19. L. HLOUSEK AND W. M. FAIRBANKS, JR., *Opt. Lett.* **8,** 322–323 (1983).
20. L. E. BERG AND L. KLYNNING, *Astron. Astrophys. Suppl.* **13,** 325–334 (1974).
21. W. W. WATSON AND W. R. FREDRICKSON, *Phys. Rev.* **39,** 765–776 (1932).
22. J. M. BROWN, M. KAISE, C. M. L. KERR, AND D. J. MILTON, *Mol. Phys.* **36,** 553–582 (1978).
23. R. A. FROSCH AND H. M. FOLEY, *Phys. Rev.* **88,** 1337–1349 (1952).
24. K. R. LEOPOLD, L. R. ZINK, K. M. EVENSON, AND D. A. JENNINGS, *J. Chem. Phys.* **84,** 1935–1937 (1986).
25. T. C. STEIMLE, C. R. BRAZIER, AND J. M. BROWN, *J. Mol. Spectrosc.* **110,** 39–52 (1985).
26. W. CHILDS AND T. C. STEIMLE, in preparation.
27. W. E. ERNST, J. KÄNDLER, C. NODA, J. S. MCKILLOP, AND R. N. ZARE, *J. Chem. Phys.* **85,** 3735–3743 (1986).
28. M. C. L. GERRY, A. J. MERER, V. SASSENBERG, AND T. L. STEIMLE, *J. Chem. Phys.* **86,** 4754–4761 (1987).
29. C. R. BRAZIER AND J. M. BROWN, *Canad. J. Phys.* **62,** 1563–1578 (1984).
30. T. C. STEIMLE, D. R. WOODWARD, AND J. M. BROWN, *J. Chem. Phys.* **85,** 1276–1282 (1986).